



Earth's Future

Supporting Information for

High Sensitivity of Compound Drought and Heatwave Events to Global Warming in the Future

Qin Zhang¹, Dunxian She^{1,2,*}, Liping Zhang^{1,2,*}, Gangsheng Wang^{1,2}, Jie Chen^{1,2}, and Zengchao Hao³

¹ State Key Laboratory of Water Resources and Hydropower Engineering Science, Wuhan University, Wuhan, 430072, China

² Institute for Water-Carbon Cycles and Carbon Neutrality, Wuhan University, Wuhan, 430072, China.

³ College of Water Sciences, Beijing Normal University, Beijing 100875, China

*Corresponding authors: Liping Zhang, zhanglp@whu.edu.cn

Dunxian She, shedunxian@whu.edu.cn

Contents of this files

Text S1 to S5

Figure S1 to S18

Table S1-S2

References

Texts

S1. Quantile Mapping (QM) bias correction method

In this study, the QM method was used to correct and minimize systematic biases in precipitation, temperature and PET from GCMs outputs due to its superiority in correcting the distribution of variables (Maraun, 2013). The general mechanism of the QM method is to find a transfer function to obtain the best fit in mapping the simulated cumulative distribution function (CDF) of the variable onto the observed CDF (Gudmundsson et al., 2012). The transfer function can be described as follow:

$$x_{bc}(t) = F_{o,h}^{-1}\{F_{m,h}[x_{m,f}(t)]\}$$

where $x_{bc}(t)$ is the bias-corrected value, $x_{m,f}(t)$ is the model output in the future period at time t , $F_{o,h}^{-1}$ and $F_{m,h}$ mean the inverse CDF corresponding to observation and model simulation, respectively, in the historical period.

We used non-parametric QM method, which match empirical CDF of observation and model output by using an interpolation method instead of assuming parametric distribution. The linear interpolation is one of non-parametric transformation methods, which have been widely employed in previous studies (Maraun, 2013; Zhang et al., 2022).

S2. FAO-PM equation

The PET is calculated using the Food and Agricultural Organization Penman–Monteith method (FAO-PM), which is a method with correctly predicting PET in a wide range of locations and climates (Allen et al. 1998). The relatively accurate and consistent performance of the FAO-PM approach in both arid and humid climates has been indicated in previous studies (Spinoni et al., 2019; Vicente-Serrano et al., 2010; Xiang et al., 2020).

The FAO-PM equation can be described as follow:

$$PET = \frac{0.408\Delta(R_n - G) + \gamma \frac{900}{T_{mean} + 273} u_2(e_s - e_a)}{\Delta + \gamma(1 + 0.34u_2)}$$

Where PET is potential evapotranspiration (mm/d), Δ is the slope of the vapor pressure curve (kPa/ $^{\circ}$ C), R_n is the net radiation at the land surface (MJ/(m 2 d)), G is the soil heat flux density (MJ/(m 2 d)), γ is psychometric constant (kPa/ $^{\circ}$ C), T_{mean} is mean daily air temperature at 2 m height ($^{\circ}$ C), u_2 is wind speed at 2 m height (m/s), e_s is saturation vapor pressure at 2 m height (kPa), and e_a is actual vapor pressure at 2 m height (kPa). The variables on the right-hand side of the equation can be calculated from the meteorology variables presented in Table 2 obtained from CMIP6 outputs.

S3. Calculating SPEI

The SPEI used for identifying droughts are constructed based on the water deficit, i.e., the difference of precipitation and PET. Firstly, the precipitation and PET at the daily scale need to be converted to the monthly scale by accumulating. Then the difference between the precipitation P and PET at the monthly scale is calculated using the following equation.

$$D_i = P_i - PET_i$$

Where D_i is the difference of precipitation and PET at month i , which is calculated at 3-month time scale. This equation provides a simple measure of the water surplus or deficit.

Considering the possibility of negative values in the D_i series, we normalize the D_i series using a three-parameter log-logistic distribution for calculation of the SPEI-3. Further the L-moment method was employed to estimate the parameters of distribution, as the method is the most robust and easy approach (Singh et al., 1993). Detailed steps on calculating SPEI can be obtained following Vicente-Serrano et al. (2010).

S4. Trend analysis

The trend of CDHW characteristics in a time series were estimated using the single linear regression based on the least squares method (Zheng et al., 2022), and the significance of trend was tested adopting the Mann-Kendall (MK) trend test (Kendall,

1975; Mann, 1945), which have been widely used in the trend detection of time series (Feng et al., 2020; Mukherjee & Mishra, 2021). A detailed description on the MK test and slope estimator is presented in the following subsection.

S4.1. Mann-Kendall test

The Mann-Kendall test is a non-parametric (i.e., distribution-free) trend test, and is used to detect the presence of linear or non-linear trends in time series data. The MK statistical variable Z can be estimated as follows:

$$S = \sum_{i=1}^{n-1} \sum_{j=i+1}^n sgn(x_j - x_i)$$

$$sgn(x_j - x_i) = \begin{cases} +1, & \text{if } x_j - x_i > 0 \\ 0, & \text{if } x_j - x_i = 0 \\ -1, & \text{if } x_j - x_i < 0 \end{cases}$$

$$Var(S) = \frac{n(n-1)(2n+5)}{18}$$

Where n is the number of sample, x_i and x_j are the data values in the time series at i and j data point, respectively, $sgn(*)$ is the sign function, $Var(S)$ denotes the variance of statistical variable S . Subsequently, the standard normal variable Z is calculated as:

$$Z = \begin{cases} \frac{S - 1}{\sqrt{Var(S)}} & \text{if } S > 0 \\ 0 & \text{if } S = 0 \\ \frac{S + 1}{\sqrt{Var(S)}} & \text{if } S < 0 \end{cases}$$

A positive value of Z indicates increasing trend of time series, while negative values imply decreasing trend. The null hypothesis is no trend of time series. When the absolute value of Z is greater than $Z_{1-\alpha/2}$ (which obtains from the standard normal cumulative distribution tables), the null hypothesis is rejected. The significance level $\alpha = 0.05$ is selected in this study.

S4.2. Slope estimator

We use a simple linear regression model to measure the linear trend of the characteristics of CDHW events in this study (Zheng et al., 2022). The slope is able to estimate as:

$$\beta = \frac{\sum_{i=1}^n (x_i - \bar{x})(y_i - \bar{y})}{\sum_{i=1}^n (x_i - \bar{x})^2}$$

Where β is the trend of data series. \bar{x}, \bar{y} denote the mean of the data series.

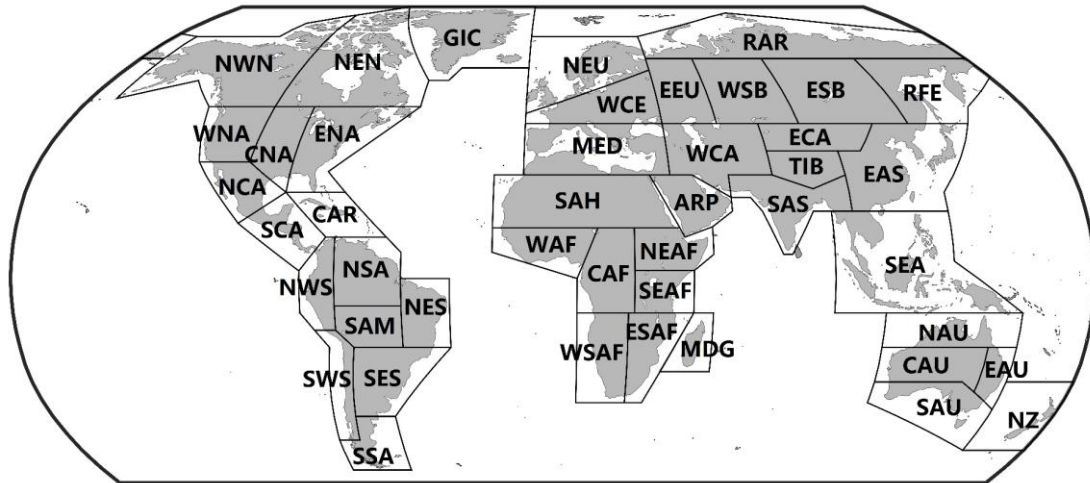
S5. Kernel Density Estimator

The kernel distribution is a nonparametric representation of the probability density function for a random variable. Comparing to a parametric distribution, we need not to make assumption about the distribution of the data. The kernel distribution is defined by a smoothing function and a bandwidth value, which control the smoothness of the resulting density curve. For any real values of x , the formula of kernel density estimator is given by:

$$\hat{f}_h(x) = \frac{1}{nh} \sum_{i=1}^n K\left(\frac{x - x_i}{h}\right)$$

Where x_i are random samples from an unknown distribution, n is the sample size, $K(\cdot)$ is the kernel smoothing function, and h is the bandwidth. The kernel smoothing function defines the shape of the curve used to generate the probability density function. Similar to a histogram, the kernel distribution builds a function to represent the probability distribution using the sample data. But unlike a histogram, which places the values into discrete bins, a kernel distribution sums the component smoothing functions for each data value to produce a smooth, continuous probability curve.

Figures



GIC: Greenland/Iceland

NWN: N.W.North-America

NEN: N.E.North-America

WNA: W.North-America

CNA: C.North-America

ENA: E.North-America

NCA: N.Central-America

SCA: S.Central-America

CAR: Caribbean

NWS: N.W.South-America

NSA: N.South-America

NES: N.E.South-America

SAM: South-American-Monsoon

SWS: S.W.South-America

SES: S.E.South-America

SSA: S.South-America

NEU: N.Europe

WCE: Western&Central-Europe

EEU: E.Europe

MED: Mediterranean

SAH: Sahara

WAF: Western-Africa

CAF: Central-Africa

NEAF: N.Eastern-Africa

SEAF: S.Eastern-Africa

WSAF: W.Southern-Africa

ESAF: E.Southern-Africa

MDG: Madagascar

RAR: Russian-Arctic

WSB: W.Siberia

ESB: E.Siberia

RFE: Russian-Far-East

WCA: W.C.Asia

ECA: E.C.Asia

TIB: Tibetan-Plateau

EAS: E.Asia

ARP: Arabian-Peninsula

SAS: S.Asia

SEA: S.E.Asia

NAU: N.Australia

CAU: C.Australia

EAU: E.Australia

SAU: S.Australia

NZ: New-Zealand

Figure S1. Geographic location and description of 44 land regions derived from IPCC AR6 (Iturbide et al., 2020).

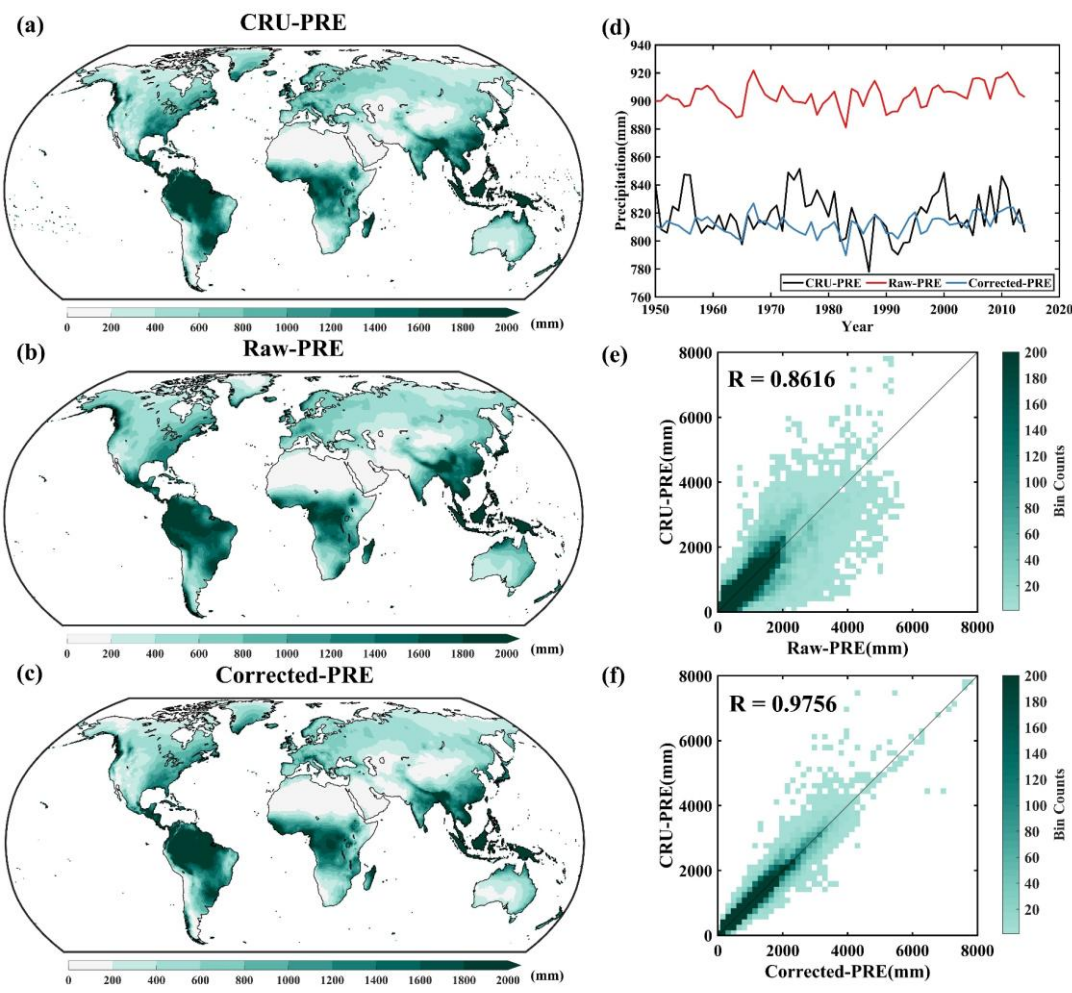


Figure S2. Same as in Figure 2 but for precipitation (PRE).

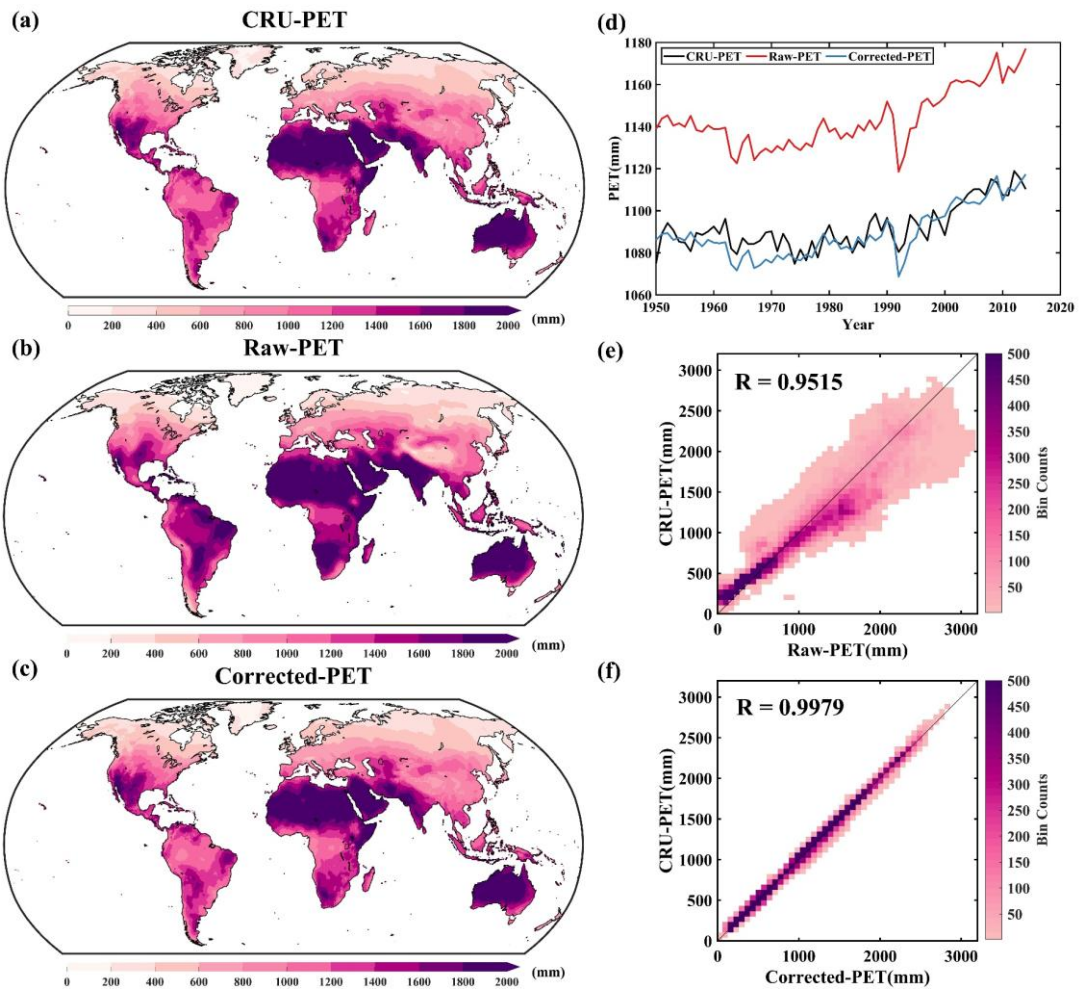


Figure S3. Same as in Figure 2 but for potential evapotranspiration (PET).

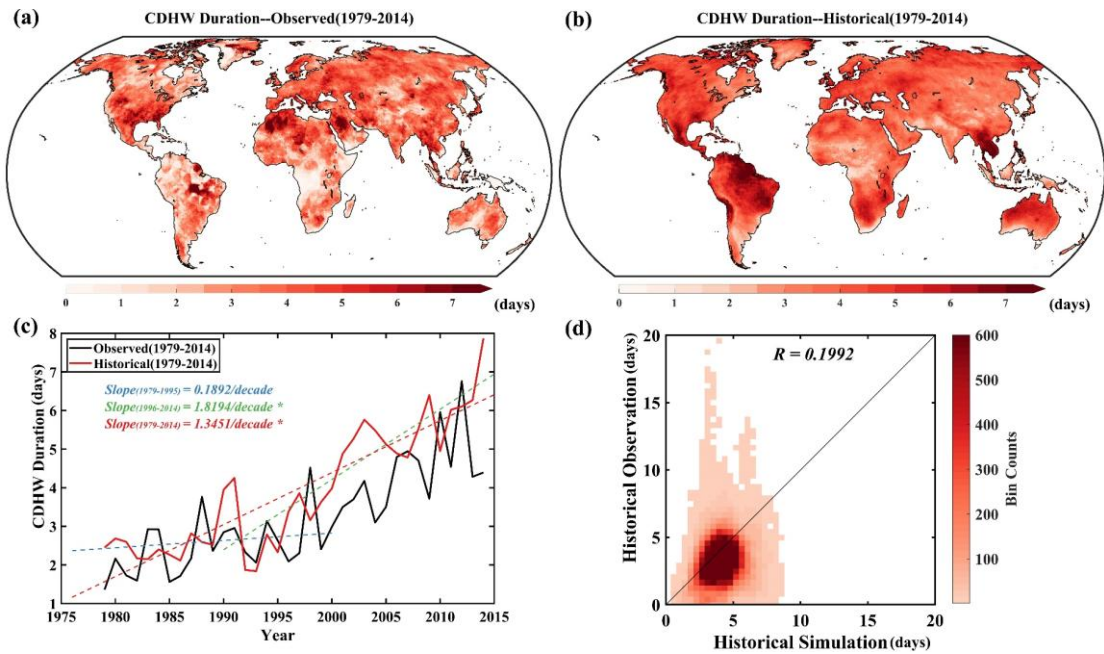


Figure S4. Same as in Figure 3 but for CDHW duration.

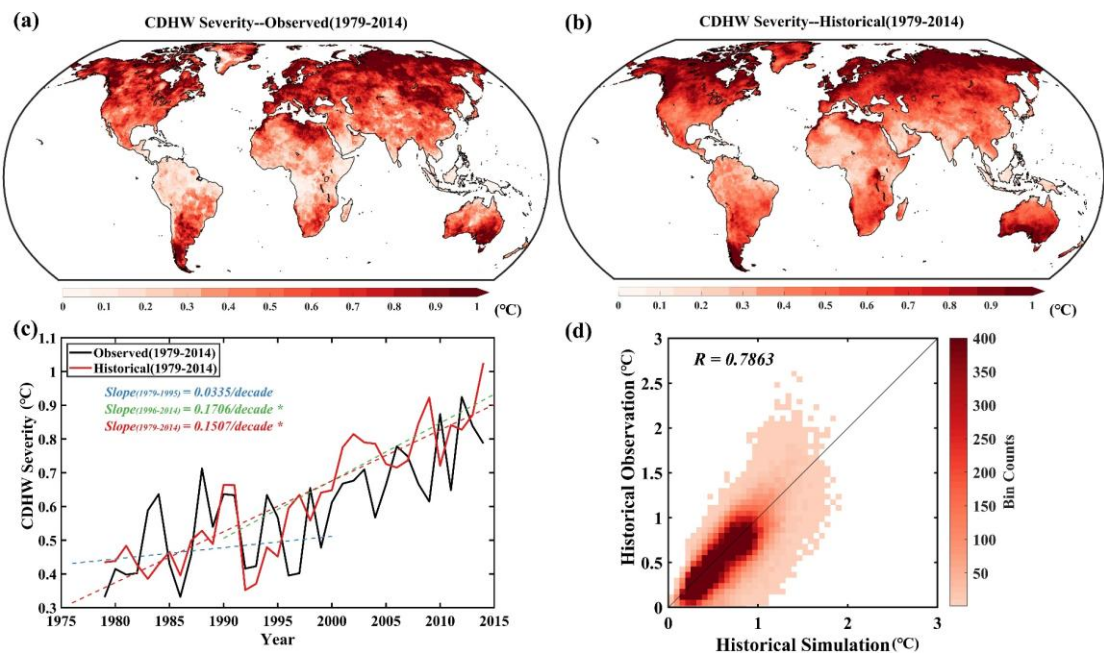


Figure S5. Same as in Figure 3 but for CDHW severity.

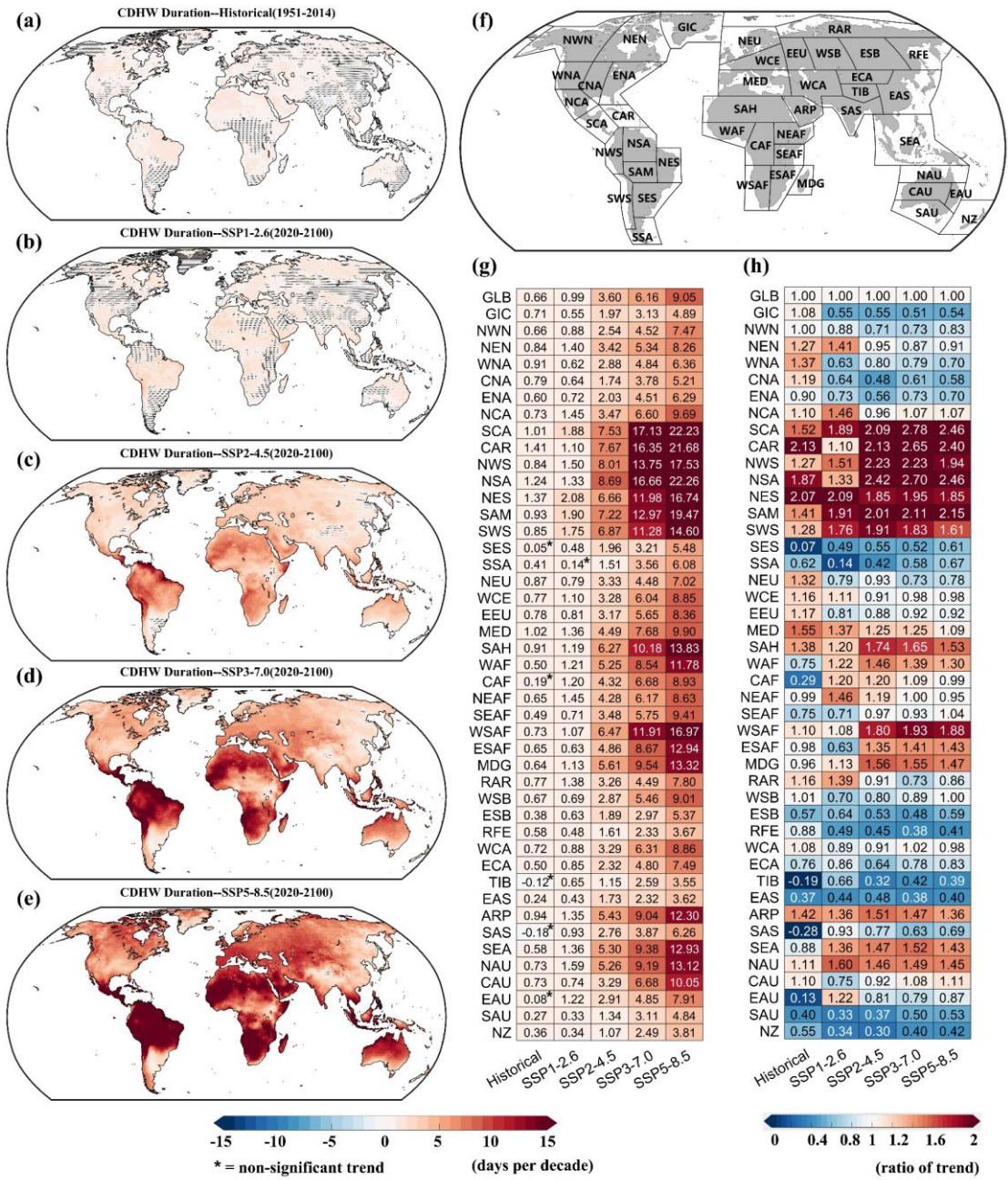


Figure S6. Same as in Figure 5 but for CDHW duration.

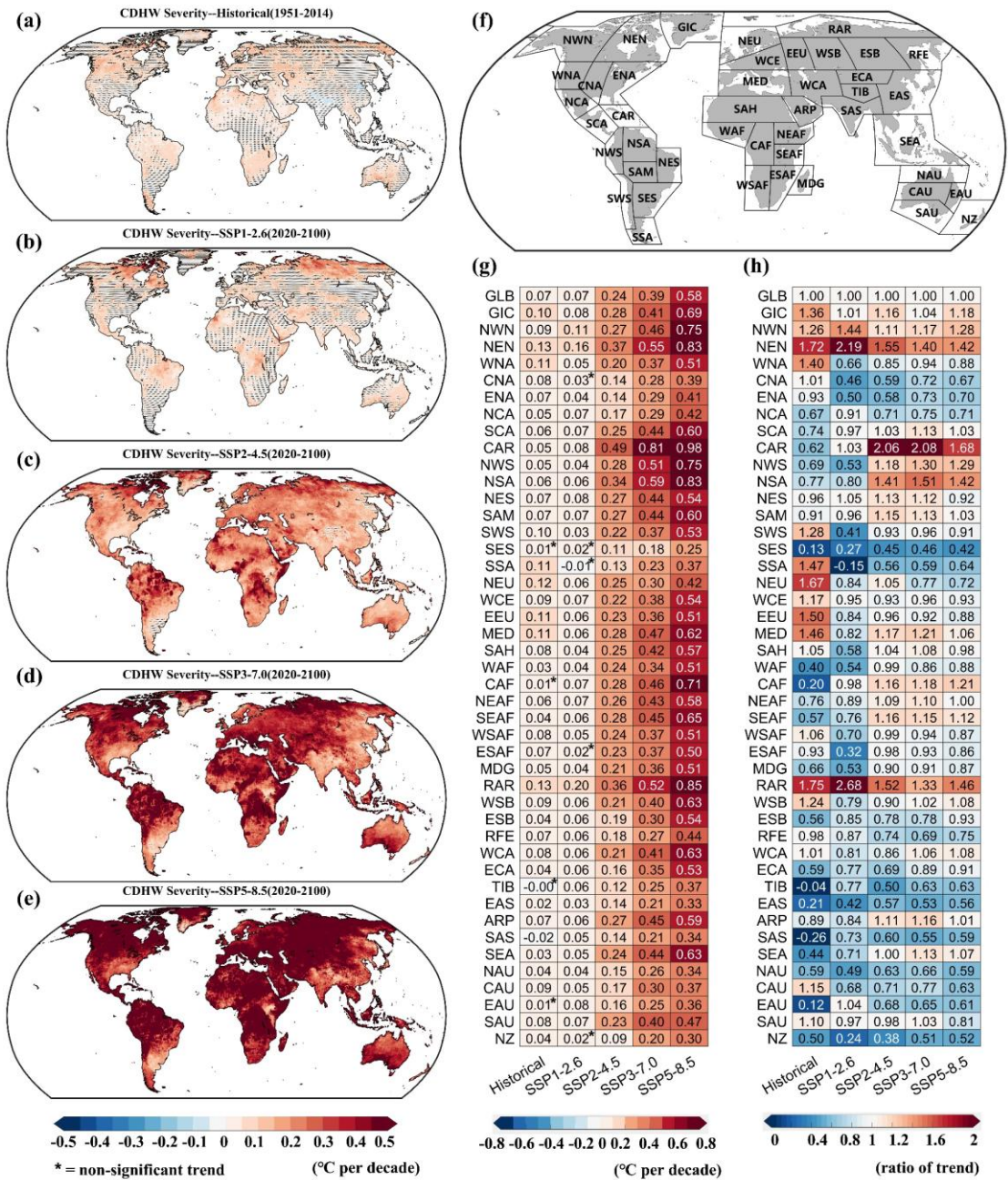


Figure S7. Same as in Figure 5 but for CDHW severity.

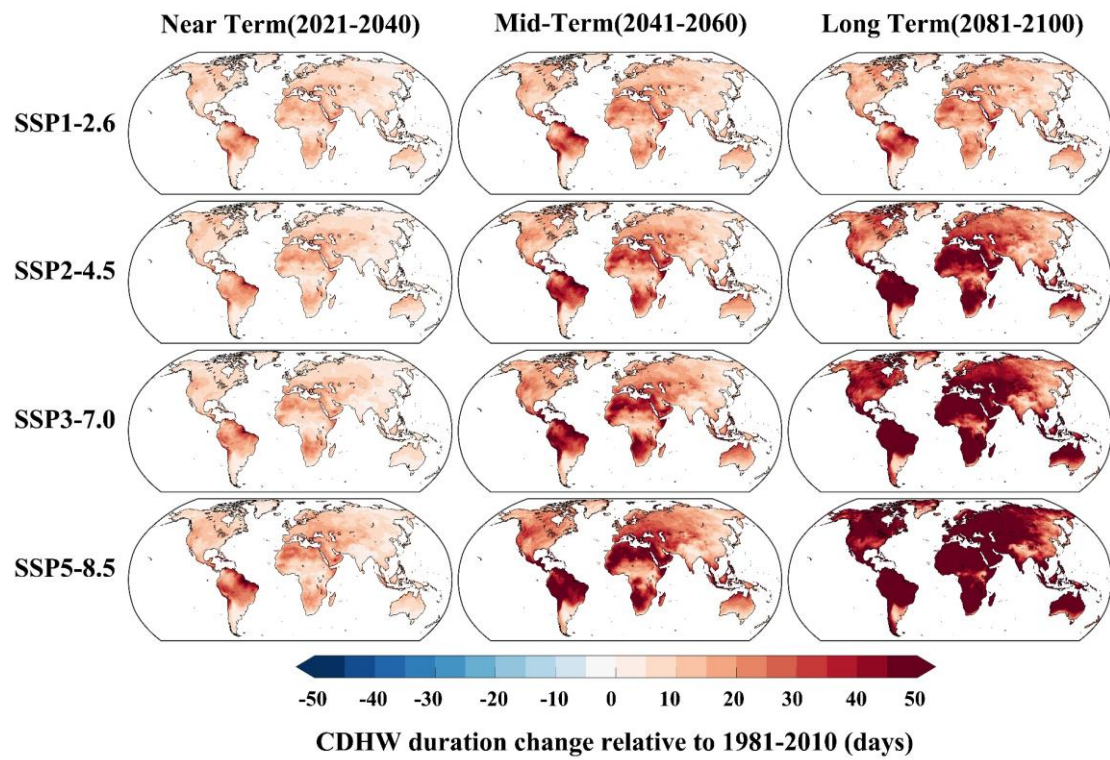


Figure S8. Same as in Figure 6 but for CDHW duration

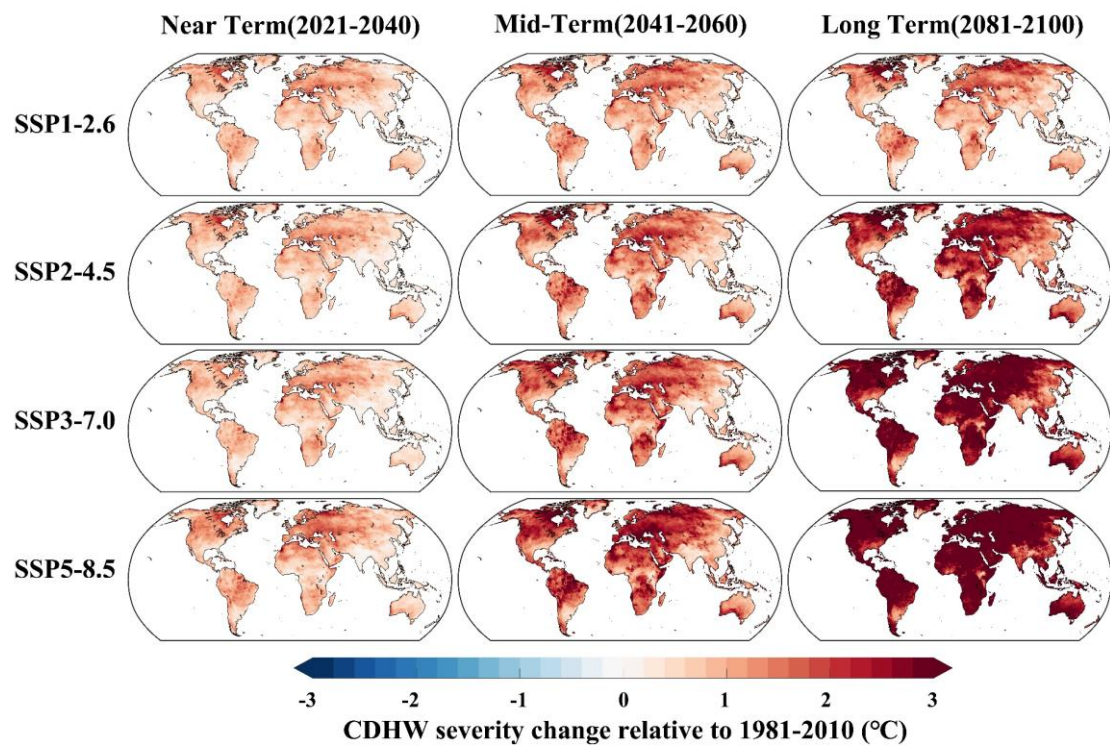


Figure S9. Same as in Figure 6 but for CDHW severity.

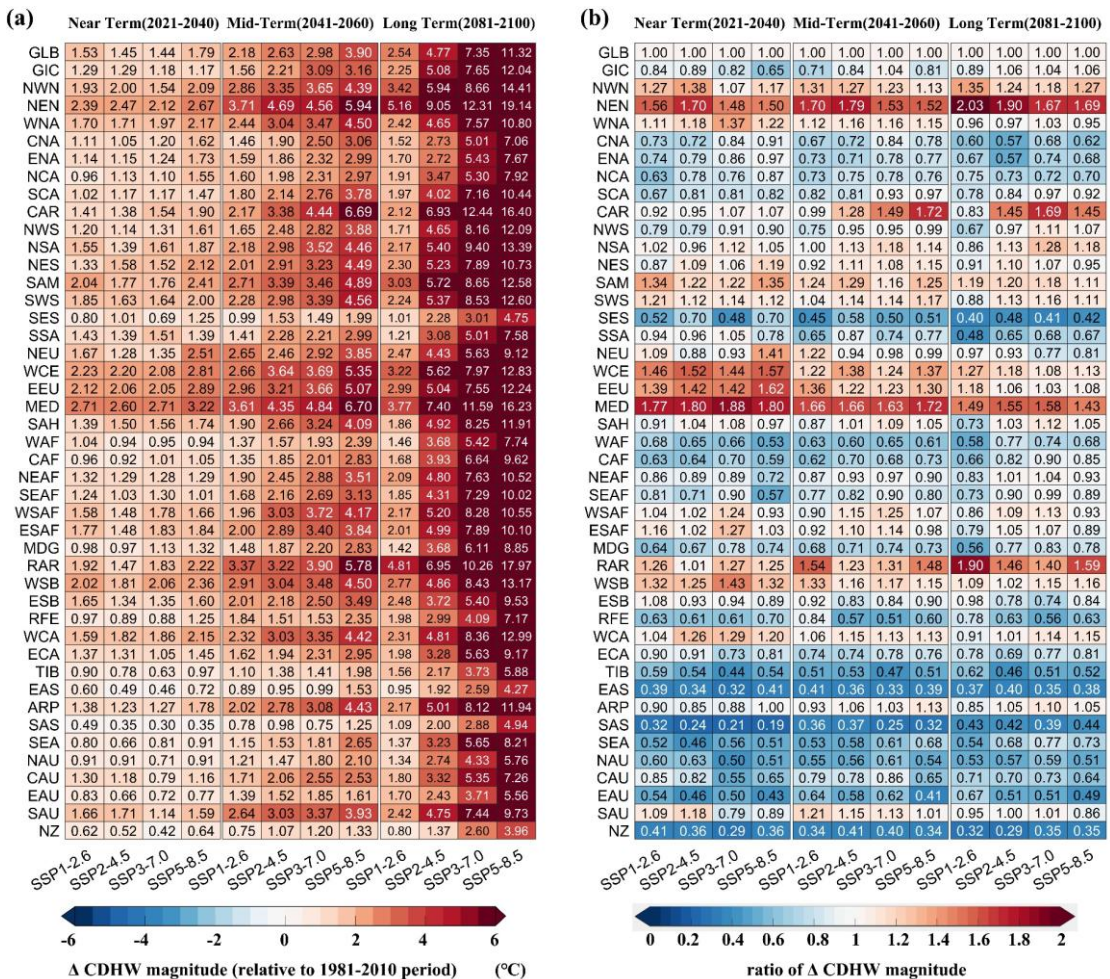


Figure S10. Regional features of CDHW mean magnitude for diverse future scenarios at near term (2021-2040), mid-term (2061-2080) and long term (2081-2100) relative to historical reference period (1981-2010). (a) Heatmap of CDHW magnitude changes for four scenarios at three terms over different regions; (b) same as (a) but for ratio of regional CDHW magnitude to global average.

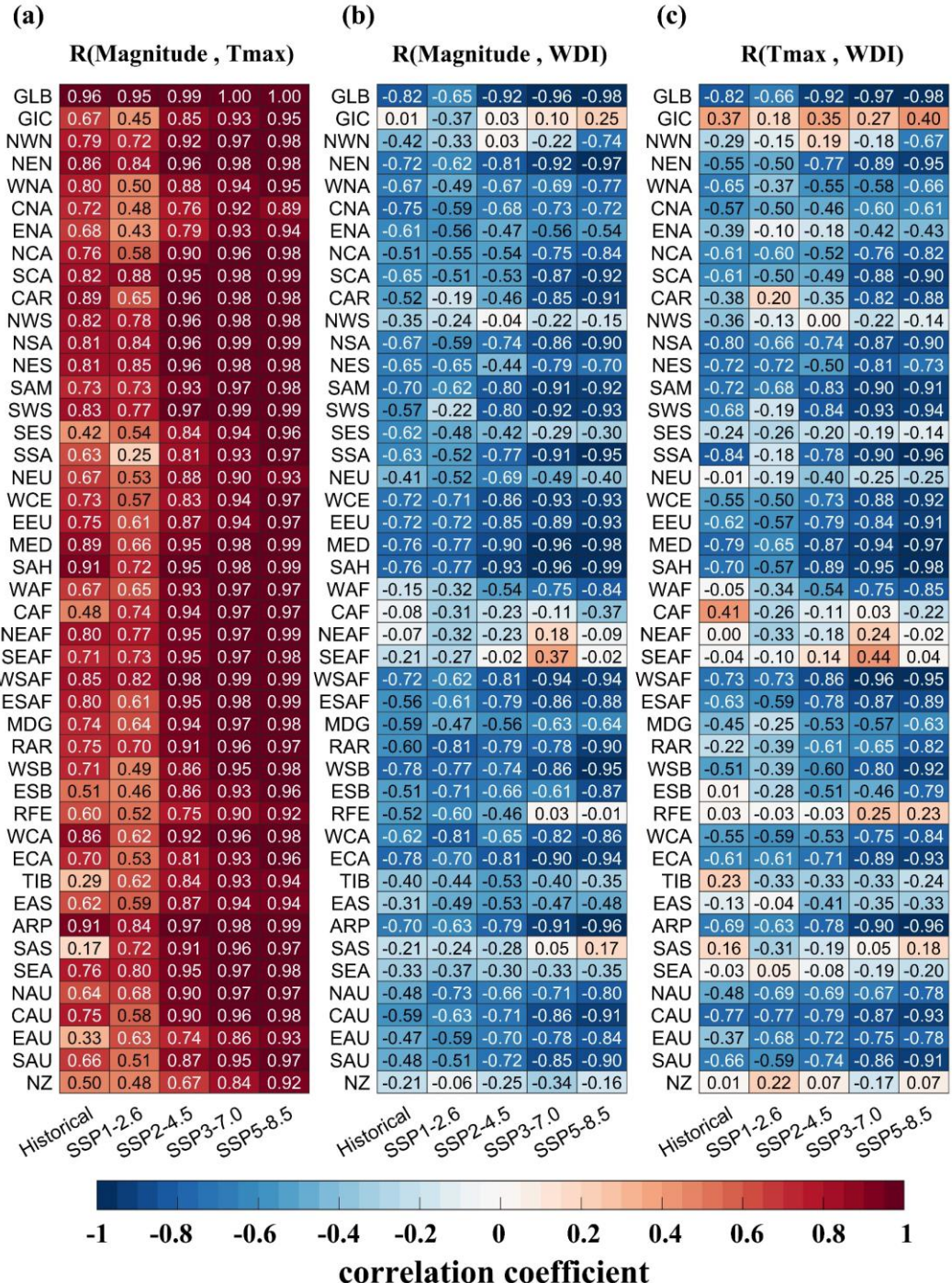


Figure S11. Heatmap of correlation coefficient for historical simulation and four future scenarios over different land regions. (a) correlation between CDHW magnitude and Tmax; (b) correlation between CDHW magnitude and WDI; (c) correlation between Tmax and WDI.

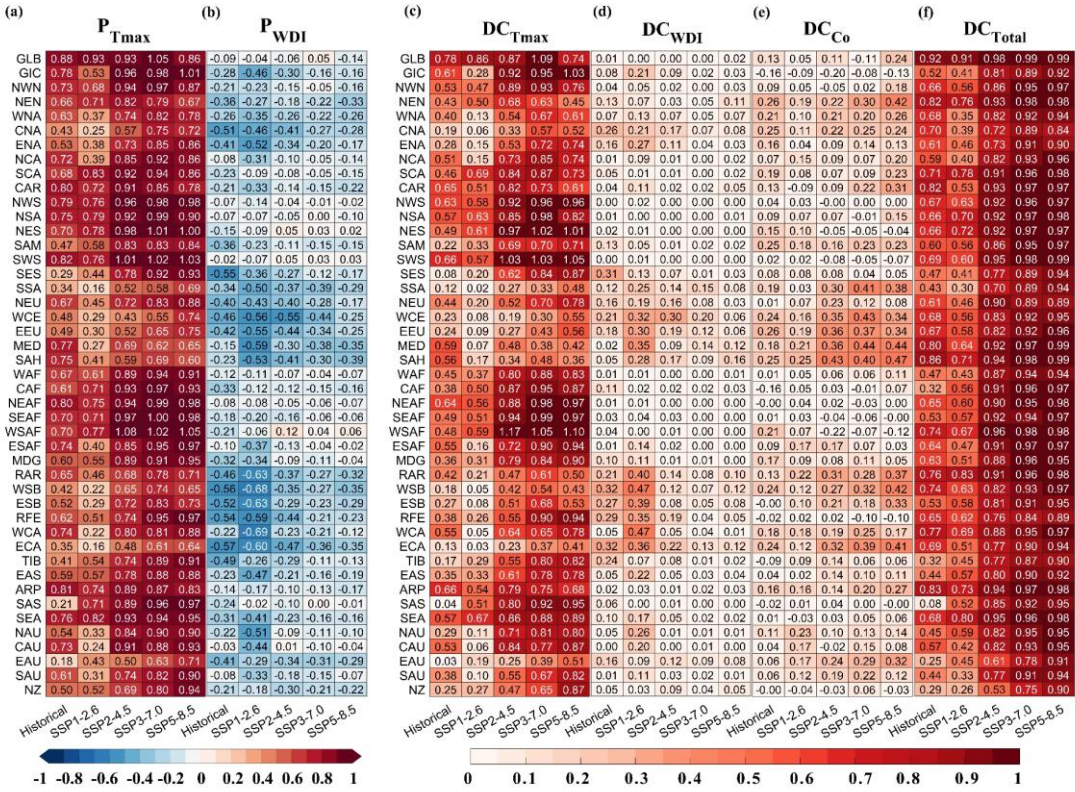


Figure S12. Heatmap of path coefficient (a-b) and determination coefficient (c-f) for historical simulation and four future scenarios over different land regions. The P_{Tmax} and P_{WDI} denote the direct effect of the annual average daily maximum temperature (Tmax) and annual total water deficit index (WDI) to CDHW magnitude, respectively. The DC_{Tmax} , DC_{WDI} , DC_{Co} and DC_{Total} represent the total determination coefficient, direct determination coefficient of Tmax and WDI, and the co-determination coefficient for Tmax and WDI.

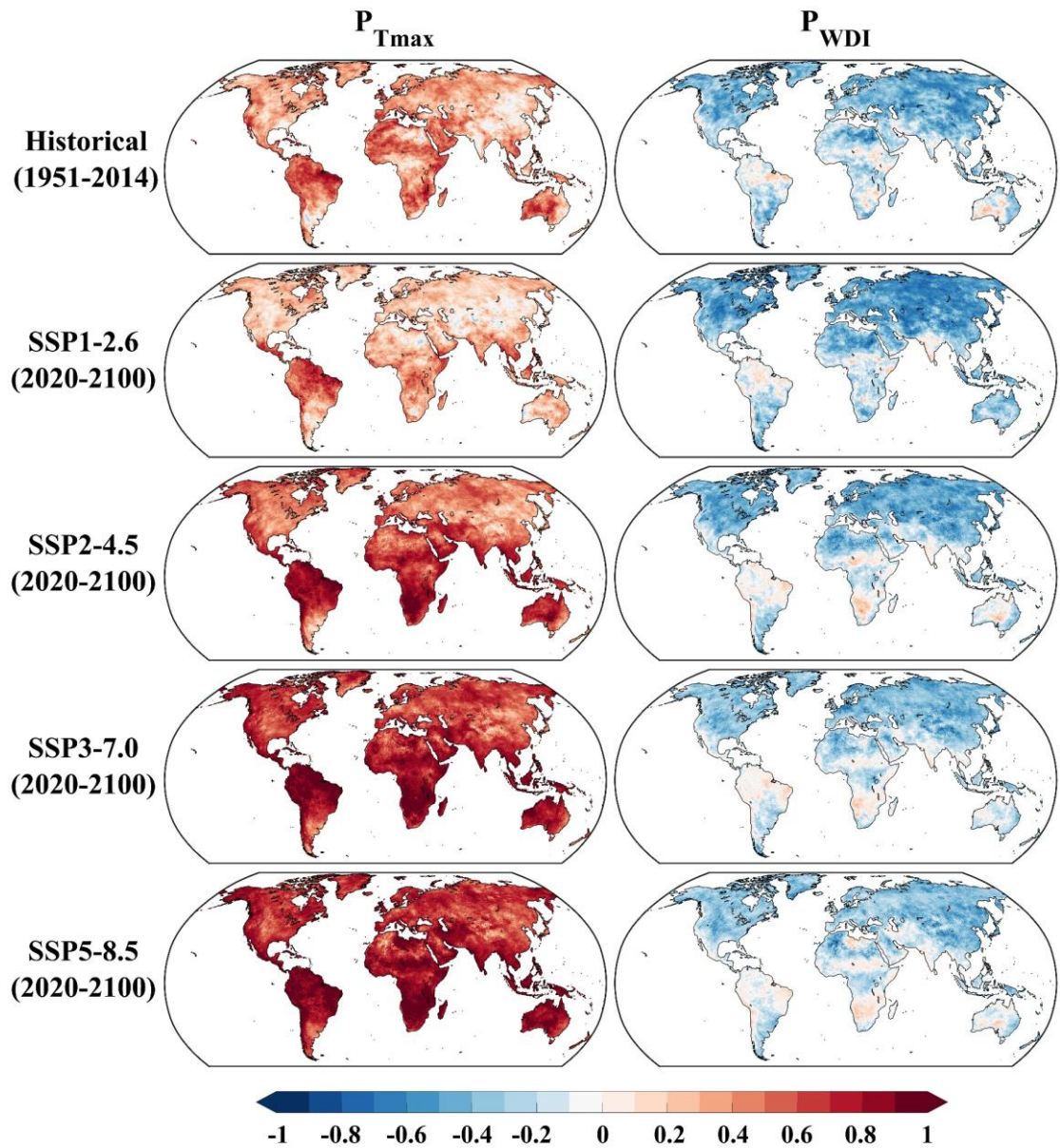


Figure S13. Spatial distributions of path coefficients including $P_{T\max}$ and P_{WDI} for CDHW magnitude under historical period, SSP1-2.6, SSP2-4.5, SSP3-7.0, SSP5-8.5, respectively.

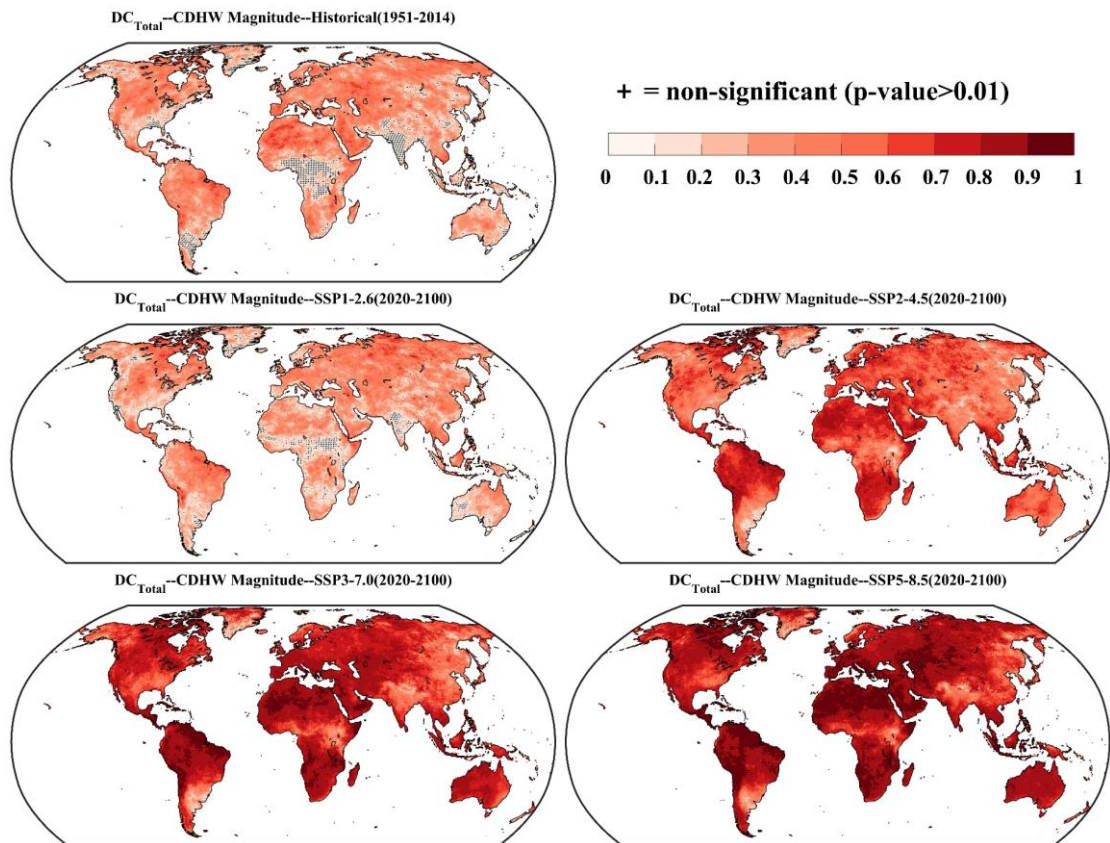


Figure S14. Spatial features of total determination coefficient for path analysis of CDHW magnitude under history and four future scenarios. The symbol “+” denotes p-value >0.01 for F test of path analysis.

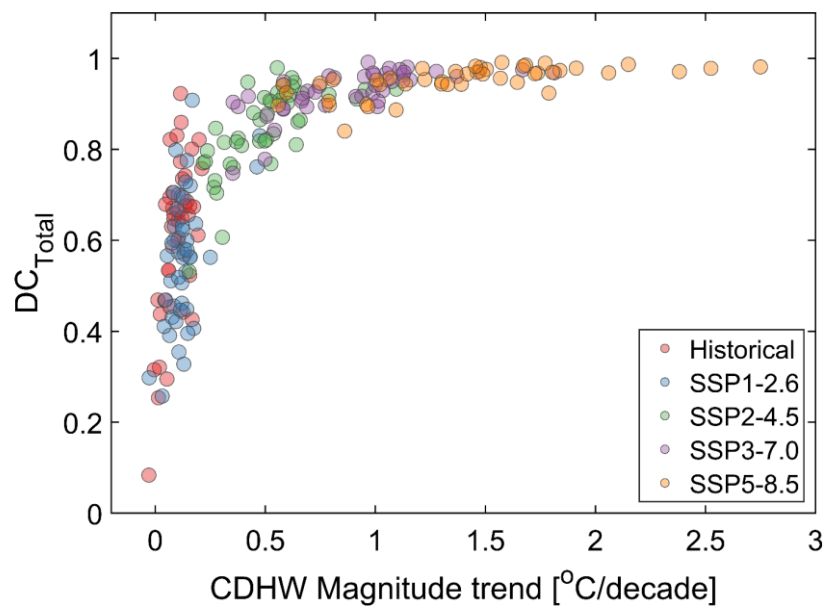


Figure S15. Relationship between total determination coefficient and CDHW magnitude trend.

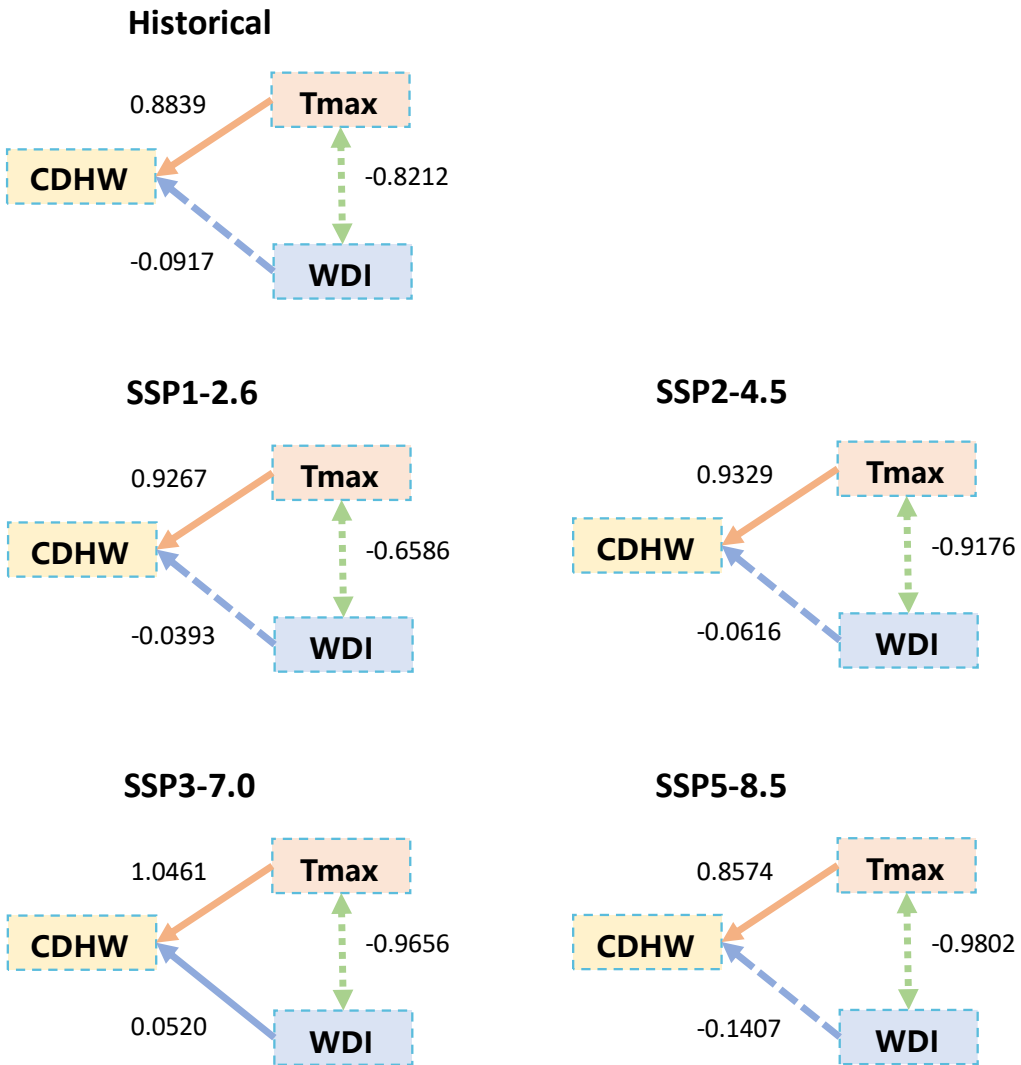


Figure S16. Path diagrams for describing the effects of daily maximum temperature (Tmax) and water deficit index (WDI) on CDHW magnitude under historical period and four future scenarios. Solid arrows represent positive effects, and dashed one are negative effect or negative correlation.

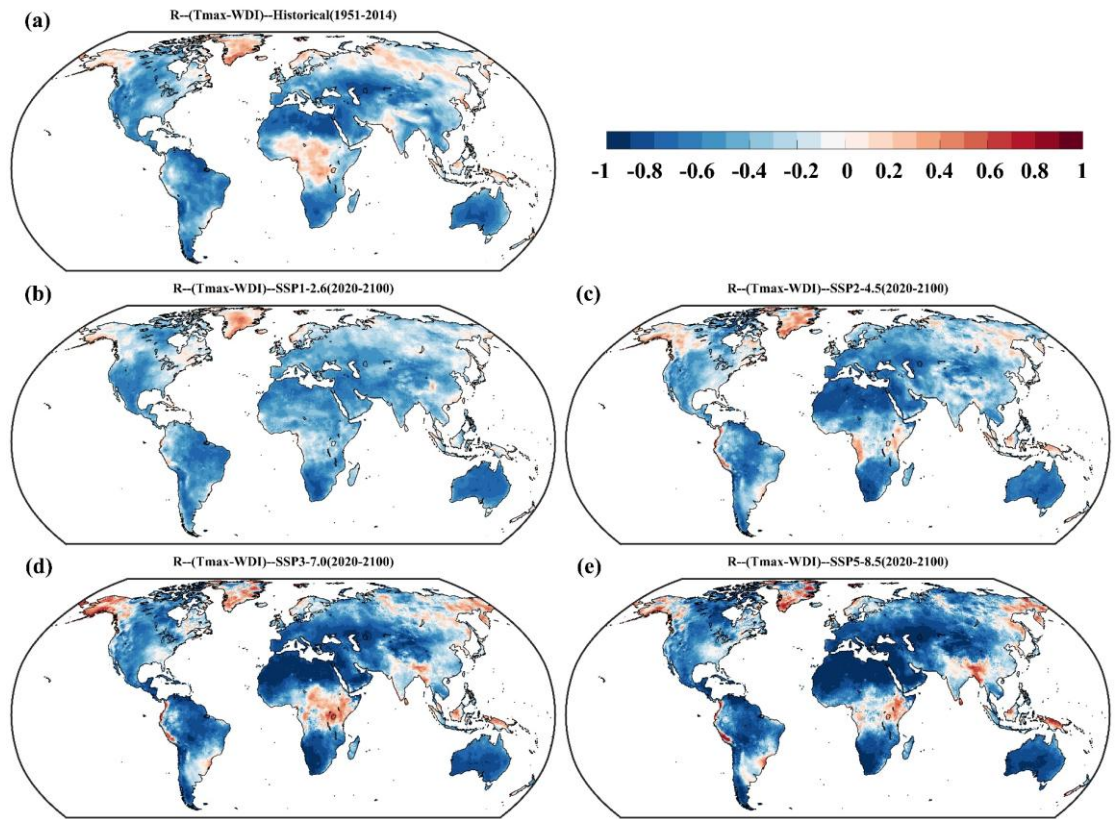


Figure S17. Spatial distributions of correlation coefficient between daily maximum temperature (Tmax) and water deficit index (WDI) under historical period and four future scenarios.

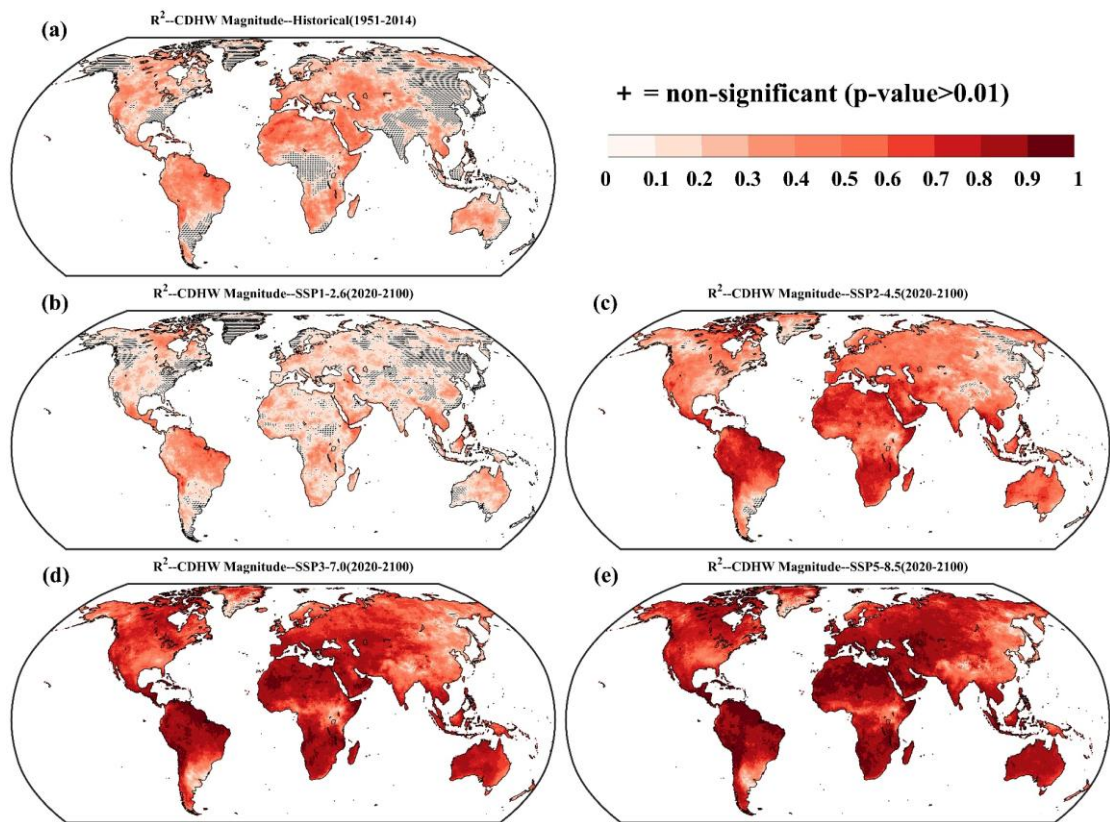


Figure S18. Spatial distributions of determination coefficient (R^2) for sensitivity analysis of CDHW magnitude under history and four future scenarios. The symbol “+” denotes $p\text{-value} > 0.01$ for F test of regression model.

Tables

Table S1. 11 Meteorological variables obtained from the GCMs outputs

| NUM | Variables | Long Name | Units |
|-----|-----------|--|------------------------|
| 1 | hurs | Near-surface relative humidity | % |
| 2 | pr | Precipitation | kg/(m ² *s) |
| 3 | psl | Sea level pressure | Pa |
| 4 | rlds | Surface downwelling longwave radiation | W/m ² |
| 5 | rlus | Surface upwelling longwave radiation | W/m ² |
| 6 | rsds | Surface downwelling shortwave radiation | W/m ² |
| 7 | rsus | Surface upwelling shortwave radiation | W/m ² |
| 8 | sfcwind | Near-surface wind speed | m/s |
| 9 | tas | Near-surface air temperature | K |
| 10 | tasmax | Daily maximum near-surface air temperature | K |
| 11 | tasmin | Daily minimum near-surface air temperature | K |

Table S2. Global average sensitivity of different CDHW characteristics to Tmax during historical and future periods.

| Scenarios | Historical | SSP1-2.6 | SSP2-4.5 | SSP3-7.0 | SSP5-8.5 |
|-----------------|------------|----------|----------|----------|----------|
| Duration (days) | 2.88* | 9.16* | 9.33* | 9.79* | 10.00* |
| Severity (°C) | 0.34* | 0.67* | 0.62* | 0.62* | 0.65* |
| Magnitude (°C) | 0.51* | 1.47* | 1.43* | 1.54* | 1.75* |

Note: The symbol “*” denotes that the results of sensitivity are statistical significant at the 0.01 significance level.

References

- Allen, R. G., Pereira, L. S., Raes, D., & Smith, M. (1998). *Crop evapotranspiration guidelines for computing crop water requirements. FAO Irrigation & drainage Paper 56*. FAO, Food and Agriculture Organization of the United Nations, Roma.
- Feng, S., Wu, X., Hao, Z., Hao, Y., Zhang, X., & Hao, F. (2020). A database for characteristics and variations of global compound dry and hot events. *Weather and Climate Extremes*, 30, 100299. <https://doi.org/10.1016/j.wace.2020.100299>
- Iturbide, M., Gutiérrez, J. M., Alves, L. M., Bedia, J., Cerezo-Mota, R., Cimadevilla, E., et al. (2020). An update of IPCC climate reference regions for subcontinental analysis of climate model data: definition and aggregated datasets. *Earth System Science Data*, 12(4), 2959–2970. <https://doi.org/10.5194/essd-12-2959-2020>
- Kendall, M. G. (1975). *Rank Correlation Methods (4th edn.)* Charles Griffin. San Francisco, CA.
- Mann, H. B. (1945). Mann Nonparametric test against trend. *Econometrica*, (13), 245–259.
- Maraun, D. (2013). Bias correction, quantile mapping, and downscaling: Revisiting the inflation issue. *Journal of Climate*, 26(6), 2137–2143. <https://doi.org/10.1175/JCLI-D-12-00821.1>
- Mukherjee, S., & Mishra, A. K. (2021). Increase in Compound Drought and Heatwaves in a Warming World. *Geophysical Research Letters*, 48(1). <https://doi.org/10.1029/2020GL090617>
- Sen, P. K. (1968). Estimates of the Regression Coefficient Based on Kendall's Tau. *Journal of the American Statistical Association*, 63(324), 1379–1389. <https://doi.org/10.1080/01621459.1968.10480934>
- Singh, V. P., Guo, H., & Yu, F. X. (1993). Parameter estimation for 3-parameter logistic distribution (LLD3) by Pome. *Stochastic Hydrology and Hydraulics*, 7(3), 163–177. <https://doi.org/10.1007/BF01585596>

- Spinoni, J., Barbosa, P., De Jager, A., McCormick, N., Naumann, G., Vogt, J. V., et al. (2019). A new global database of meteorological drought events from 1951 to 2016. *Journal of Hydrology: Regional Studies*, 22, 100593.
<https://doi.org/10.1016/j.ejrh.2019.100593>
- Vicente-Serrano, S. M., Beguería, S., & López-Moreno, J. I. (2010). A Multiscalar Drought Index Sensitive to Global Warming: The Standardized Precipitation Evapotranspiration Index. *Journal of Climate*, 23(7), 1696–1718.
<https://doi.org/10.1175/2009JCLI2909.1>
- Xiang, K., Li, Y., Horton, R., & Feng, H. (2020). Similarity and difference of potential evapotranspiration and reference crop evapotranspiration – a review. *Agricultural Water Management*, 232(January).
<https://doi.org/10.1016/j.agwat.2020.106043>
- Zhang, Q., Gan, Y., Zhang, L., She, D., Wang, G., & Wang, S. (2022). Piecewise-quantile mapping improves bias correction of global climate model daily precipitation towards preserving quantiles and extremes. *International Journal of Climatology*, (December 2021), 1–19. <https://doi.org/10.1002/joc.7687>
- Zheng, H., Miao, C., Li, X., Kong, D., Gou, J., Wu, J., & Zhang, S. (2022). Effects of Vegetation Changes and Multiple Environmental Factors on Evapotranspiration Across China Over the Past 34 Years. *Earth's Future*, 10(4), 1–16.
<https://doi.org/10.1029/2021EF002564>